ELSEVIER

Journal of Hazardous Materials B:63 (1998) 163–177

Journal of Hazardous Materials

Speciation of silver in cementitious environment

M. Yousuf, A. Mollah [1], Jie Liang, David L. Cocke [*]

Gill-Chair of Analytical Chemistry, P.O. BOX 10022, Lamar University, Beaumont, TX 77710, USA

Received 29 September 1995; revised 23 July 1998; accepted 25 July 1998

Abstract

Speciation of silver in cementitious environments has been investigated by Fourier Transform Infrared Spectroscopy (FT-IR), X-ray diffraction (XRD) and scanning electron microscopy/energy dispersive spectroscopy (SEM/EDS). The results of this study have delineated that Ag_2O, Ag_2CO_3 and AgCl are formed in highly alkaline environments in the cement system. Scanning electron microscopic examination of the hydrated cement treated with Ag^+ (OPC-V/Ag) revealed the presence of clusters of AgCl in the Ag-doped sample. The mechanisms of formations of these compounds are discussed.

Keywords: Silver; Speciation; Solidification/stabilization; Fourier transform infrared spectroscopy; Scanning electron microscopy/energy dispersive spectroscopy; X-ray diffraction

1. Introduction

Solidification/Stabilization (S/S) of toxic metals has received considerable attention, since the presence of these metals in the environment causes deleterious effects on human health and aquatic wild life. Silver is considered a toxic chemical according to Section 313 of the Emergency Planning and Community Right-to-Know Act of 1986 [1]. It is introduced into the environment through natural geological sources as well as anthropogenic activities involving the uses of photographic materials, electroplating materials, conductors, dental alloys, solder and brazing alloys, paints, jewelry, silverware, coinage, and mirror production. It is also used as water disinfectants and antibacterial agents since it can interfere with essential metabolic processes in the bacterial cell [2]. According to USEPA Ambient Water Quality Criteria for silver for

[*] Corresponding author. Tel.: +1 409 880 1862; fax: +1 409 880 8374; e-mail: cockedl@hal.lamar.edu
[1] Visiting Professor, Department of Chemistry, University of Dhaka, Bangladesh.

0304-3894/98/$ - see front matter
PII: S0304-3894(98)00194-0

freshwater aquatic life, the concentration (μg/l) of total recoverable silver should not exceed the numerical value given by $e^{(1.72[\ln(\text{hardness})]-6.25)}$ at any time [3]. The available data indicates that chronic toxicity to fresh water aquatic life may occur at concentrations as low as 0.12 μg/l. For salt water aquatic life, the concentration of total recoverable silver should not exceed 2.3 μg/l at any time [3].

The most prevalent S/S practice in the USA and many European countries is the use of cement and pozzolan-based materials for immobilization of wastes containing toxic metals. Most of the work done to date have been summarized in recent reviews and books [4–8]. However, in a continuing research program to characterize the speciation of priority metal pollutants in cement-based S/S materials, we have investigated the S/S of silver using Portland cement type-V (henceforth OPC-V).

2. Experimental

Silver doped samples were prepared by mixing 10% (w/w) of Ag^+ with sulfate resisting OPC-V (Texas Industries). Deionized water was used to prepare samples with a water/cement ratio (w/c) of 0.35. Samples were cured in an ambient atmosphere under normal laboratory conditions. Analytical grade $AgNO_3$ (99.9% pure) received from Aldrich Chem. was used as a source of Ag^+ ions. Experimental details for the preparation of samples and the methods of analyses by XRD, FT-IR and SEM/EDS have been reported elsewhere [9–11]. However, the methods of analyses are briefly given below.

2.1. FT-IR

The FT-IR spectra were recorded by Nicholet FT-IR 500 instrument using KBr pellets. The spectra were recorded over the range 400–4000 cm^{-1} with 2 cm^{-1} resolution. Usually 32 scans were recorded.

2.2. XRD

The XRD analyses were performed using Cu K_α radiation (35 kV and 25 mA) on a scintag XDS 2000 diffractometer equipped with a graphite monochromator. The samples were pulverized to a fine, homogeneous powder using a mortar and pestle and then filled into a ring-shaped hollow aluminum holder. The holder contained glass slide that had a rectangular hollow area for holding the powder samples. The glass slide smoothly pressed the sample into a rectangular area. The XRD scan was run at 0.02 0 steps and 15 s counting time.

2.3. SEM / EDS

The SEM/EDS analyses were carried out on a JOEL-6400 scanning electron microscope (SEM) equipped with a Tracor-Northern Series 2 EDS system with a germanium detector and diamond window. Prior to analysis, the samples were dry-cut

using Isomet low speed saw with a diamond studded blade. The sample slices were mounted using double-sided tape.

3. Results and discussion

3.1. XRD

The data obtained from XRD analyses of silver-doped cement are presented in Table 1, and the corresponding powder diffraction patterns of dry clinker (A), hydrated cement (B) and silver-doped cement (C) are shown in Fig. 1. Alite (Ca_3SiO_5) and belite (Ca_2SiO_4) upon contact with water produce portlandite $Ca(OH)_2$ (20–25%) and amorphous calcium–silica–hydrate, C–S–H, (60–70%). Since the C–S–H is amorphous, it cannot be detected by XRD technique. The XRD peaks corresponding to ettringite appear at 9.73, 5.61 and 3.88 Å [12]. The peak that appears at 9.745 Å (Fig. 1) is attributed to ettringite.

The peak corresponding to $CaCO_3$ comes from the reactions between atmospheric CO_2 and C–S–H or CH [13]. The CH and $CaCO_3$ peaks are absent in the diffractogram of dry clinkers.

A close examination of the diffractogram (Fig. 1) of OPC-V/Ag in the region 3.00–1.70 Å clearly indicates two shoulders on either side of the peak centered at 2.696 Å, and a weak peak at 2.78 Å. These peaks are considered due to either Ag_2O or Ag_2CO_3. The XRD data for Ag_2O, Ag_2CO_3 and AgCl obtained from the literature [12]

Table 1
XRD data for Ag-doped Portland cement Type-V

2θ	d (Å)	% I_p[a]	Phase[b]
9.0	9.745	57	E
10.2	8.445	47	
18.0	4.906	91	CH
22.0	4.074	40	
24.2	3.655	54	fer
29.0	3.036	46	ali
32.0	2.783	40	AC/ACl/AO ali, bel, fer
33.0	2.696	99	AC/ACl/AO ali, bel
34.0	2.620	100	AC/ACl/AO CH
38.4	2.338	36	ali
41.0	2.183	29	ali
47.0	1.924	60	CH/fer
51.0	1.794	33	CH
54.5	1.685	28	CH
56.0	1.653	25	ali

[a] I_p = Relative peak intensity.
[b] E = Ettringite, CH = $Ca(OH)_2$, ali = alite, bel = belite, fer = ferrite, C = $CaCO_3$, AC = Ag_2CO_3, ACl = AgCl, and AO = Ag_2O.

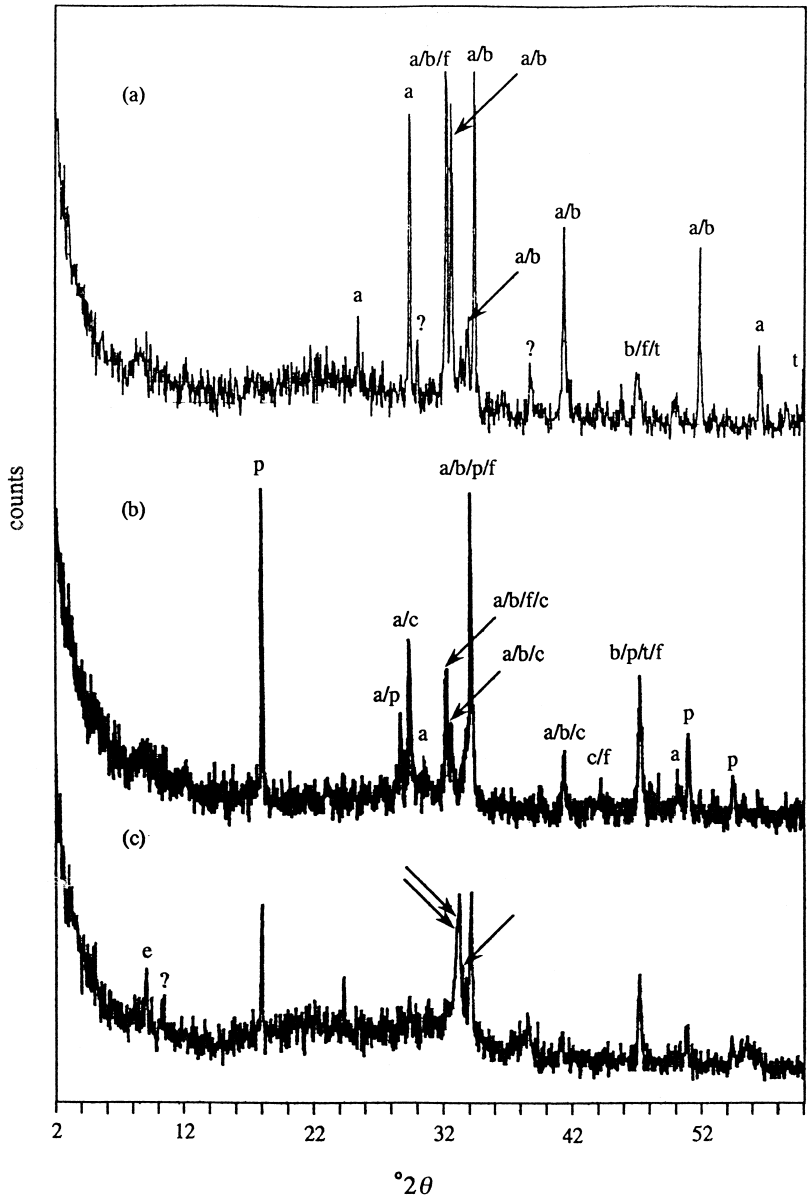

Fig. 1. XRD of (a) dry clinkers; (b) hydrated OPC-V and (c) OPC-V/Ag.

and the observed XRD peaks from the present experiment are presented in Table 2. Although it is rather difficult to make any definitive conclusions based on these peaks only, the XRD data combined with FT-IR and SEM/EDS analyses of the OPC-V/Ag spur us to conclude that Ag_2O, Ag_2CO_3 and AgCl are actually formed in the

Table 2
X-ray powder diffraction data of silver species from literature and results from OPC-V/Ag sample in the present experiment

Compounds	d (Å)[a]		
Ag_2O	2.73	2.37	1.67
AgCl	2.77	1.96	3.2
Ag_2CO_3	2.66	2.74	2.27
OPC-V/Ag	2.620	2.696	1.924
observed	3.036	2.783	1.794

[a] Phase was determined from J.C.P.D.S. index [12].

OPC-V/Ag system. Further discussion to firmly establish the formation of these compounds will be given in Section 3.

3.2. FT-IR

The FT-IR transmission spectra of dry clinkers, hydrated OPC-V and silver-doped OPC-V (OPC-V/Ag) in the region 400–1600 cm^{-1} are shown in Fig. 2, and the spectral data (400–4000 cm^{-1}) is presented in Table 3. The spectrum of dry clinkers shows that there are three major vibrational bands at 930, 522 and 451 cm^{-1}, in agreement with our previous reports [9,14]. These bands are assigned to Si–O asymmetric stretching vibration (υ_3) of silicate tetrahedra, Si–O out-of-plane bending vibration (υ_2) and Si–O in-plane bending (υ_4) vibrations, respectively. The bands between 1100–1160 cm^{-1} are due to S–O vibrations (υ_3) of the sulfate (SO_4^{2-}). The SiO_4^{4-} vibrational bands undergo significant changes upon hydration of OPC-V, because cement particles react with water to produce a new silica phase [15]. The Si–O stretching band is now shifted to a higher frequency at 950 cm^{-1} due to condensation of the orthosilicates.

The intensity of the out-of-plane bending vibration of the SiO_4^{4-} group which appears at 522 cm^{-1} has been reduced, while that of the in-plane bending vibration of SiO_4^{4-} group (452 cm^{-1}) has been correspondingly increased. The shifting of the Si–O stretching vibration to higher frequency and the relative change of the intensities of the in-plane and out-of-plane bending vibrations are diagnostic of the polymerization of the SiO_4^{4-} units in the cement system to form C–S–H [15,16] phase. Since the out-of-plane deformation (υ_4) is restricted with hydration and increased linkage between Si–O–Si units, the υ_3 of SiO_4^{4-} vibrations in hydrated samples has a reduced intensity, and appears at a higher frequency as compared with that of dry clinkers. An increased intensity of the υ_2 vibration is caused by a decrease in the freedom of motion that occurs upon polymerization of the orthosilicate units. The sulfate band (υ_3) which appears between 1100–1140 cm^{-1} in the dry clinkers has now been obscured by shifting of the Si–O stretching band due to polymerization.

The broad and strong band in the region 3400–3700 cm^{-1} is due to symmetric and asymmetric (υ_1 and υ_3) stretching vibrations of O–H in water molecules of the hydrated

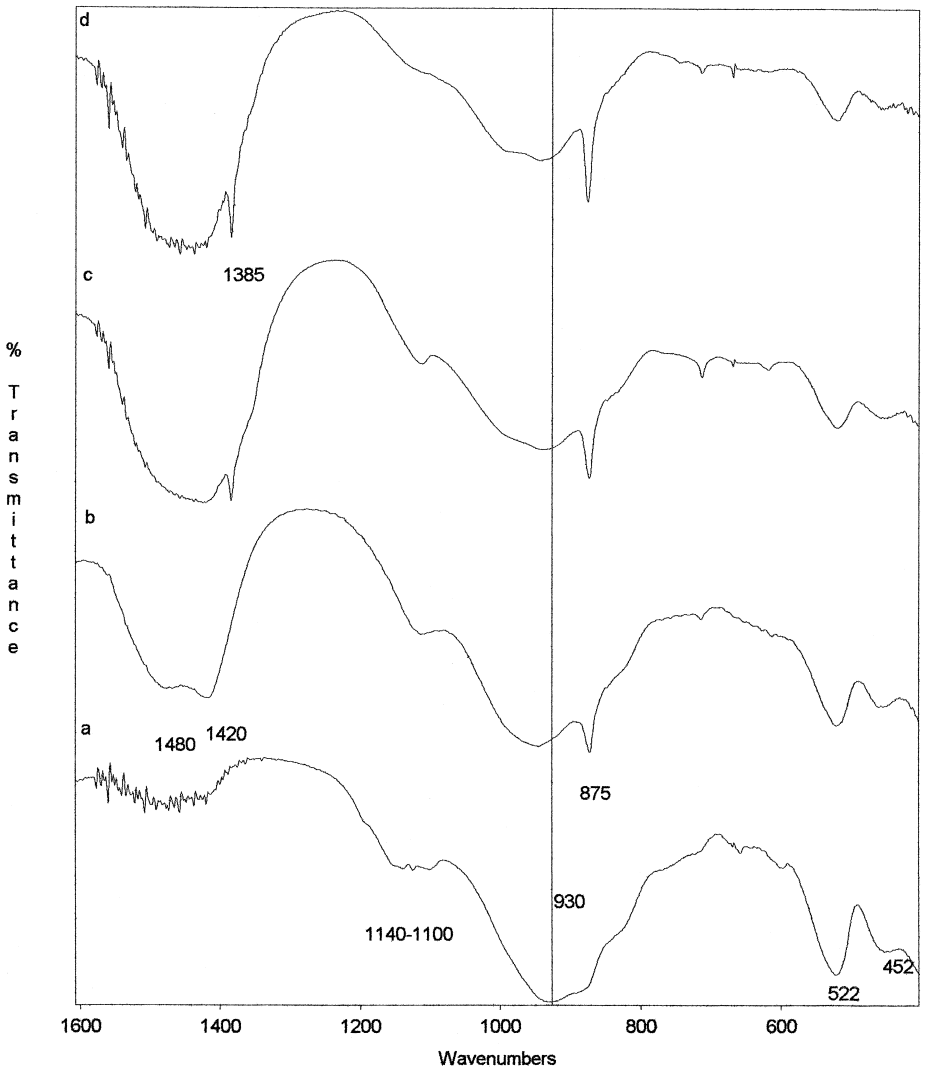

Fig. 2. FT-IR spectra of (a) dry clinkers; (b) hydrated OPC-V; (c) OPC-V/Ag (28 days) and (d) OPC-V/Ag (1 year) samples.

OPC-V, while the sharp band at 1653 cm^{-1} is given by the H–O–H bending vibration (υ_2) of an adsorbed water molecule [15,17].

The CO_3^{2-} regions exhibit bands between 1385–1437 cm^{-1} and at 873 cm^{-1}. The effect of Ag^+ on the hydration of OPC-V can be seen from Fig. 2. The stretching vibration of the SiO_4^{4-} group (υ_3) in OPC-V/Ag sample appears at 960 cm^{-1}, while the same peak in the only cement sample appears at 950 cm^{-1}. The SiO_4^{4-} stretching band in the Ag-doped sample is comparatively stronger and appears at a higher wavenumber region than either of the dry cement or hydrated cement. The band due to

Table 3
FT-IR data for dry clinker, hydrated OPC, air-cured OPC-V/Ag

Band assignments	Dry clinker (cm^{-1})	OPC-V paste (w/c = 0.35) (cm^{-1})	10% OPC-V/Ag[a] (w/c = 0.35) (cm^{-1})
υ_3 SiO_4^{4-}	930	950	960
υ_4 SiO_4^{4-}	522	521	519
υ_2 SiO_4^{4-}	452	453	459
υ_3 SO_4^{2-}	1100–1140	1111	1115
υ_4 SO_4^{2-}	668	669	667
$\upsilon_1 + \upsilon_3$ H_2O		3404–3634	3404–3634
υ_2 H_2O	–	1653	1653
υ OH^-	–	3642	–
υ_3 CO_3^{2-}	–	1385–1437	1385–1437
υ_2 CO_3^{2-}	–	873	873
υ_1 NO_3^{2-}	–	–	1384
			742

OPC = Ordinary Portland cement.
[a]A one year old sample gave almost identical spectrum.

out-of-plane vibration appearing at 519 cm^{-1} now appears with much reduced intensity. The intensity of the in-plane bending vibration of the SiO_4^{4-} group centered at 459 cm^{-1} has been correspondingly enhanced. These vibrational changes are indicative of the participation of Ag^+ in the hydration process. Two bands appearing at 1384 and 742 cm^{-1} are due to NO_3^{1-} group which comes from $AgNO_3$ used as the source of Ag^+.

The reactions of atmospheric CO_2 with $Ca(OH)_2$ in Ag-doped cement result in the strong carbonate bands appearing between 1300–1500 cm^{-1} and 873 cm^{-1}. The sharp band appearing at 3642 cm^{-1} is due to the O–H stretch of $Ca(OH)_2$, which provide further evidence that $Ca(OH)_2$ and C–S–H have reacted with atmospheric CO_2 to form $CaCO_3$.

3.3. SEM / EDS

A typical SEM micrograph ($\times 1000$) of OPC-V blank and a representative EDS spectrum are presented in Fig. 3. The SEM image shows that cement paste consists of layers of thin platy hexagonal $Ca(OH)_2$ crystals surrounded by bright flaky materials. The flaky materials are amorphous in nature without any definite structure, and composed of mainly C–S–H gels. Micro-structural examinations of the SEM images do not indicate the presence of either ettringite or monosulfate, since the sample was not analyzed at the early stage of hydration. An SEM image of OPC-V/Ag (area 1) and an EDS spectrum of the corresponding area are presented in Fig. 4. The morphology of this sample is more or less similar except that it shows a more flaky type (C–S–H) gel than that of the OPC-V blank, and no clear platy hexagonal $Ca(OH)_2$ crystals are observed in this area as in the OPC-V blank (Fig. 3). It thus indicates that the addition of silver did not strongly affect the cement morphology and micro-structure. The elements identified from EDS scans are: calcium, silicon, oxygen, aluminum, carbon, potassium (trace),

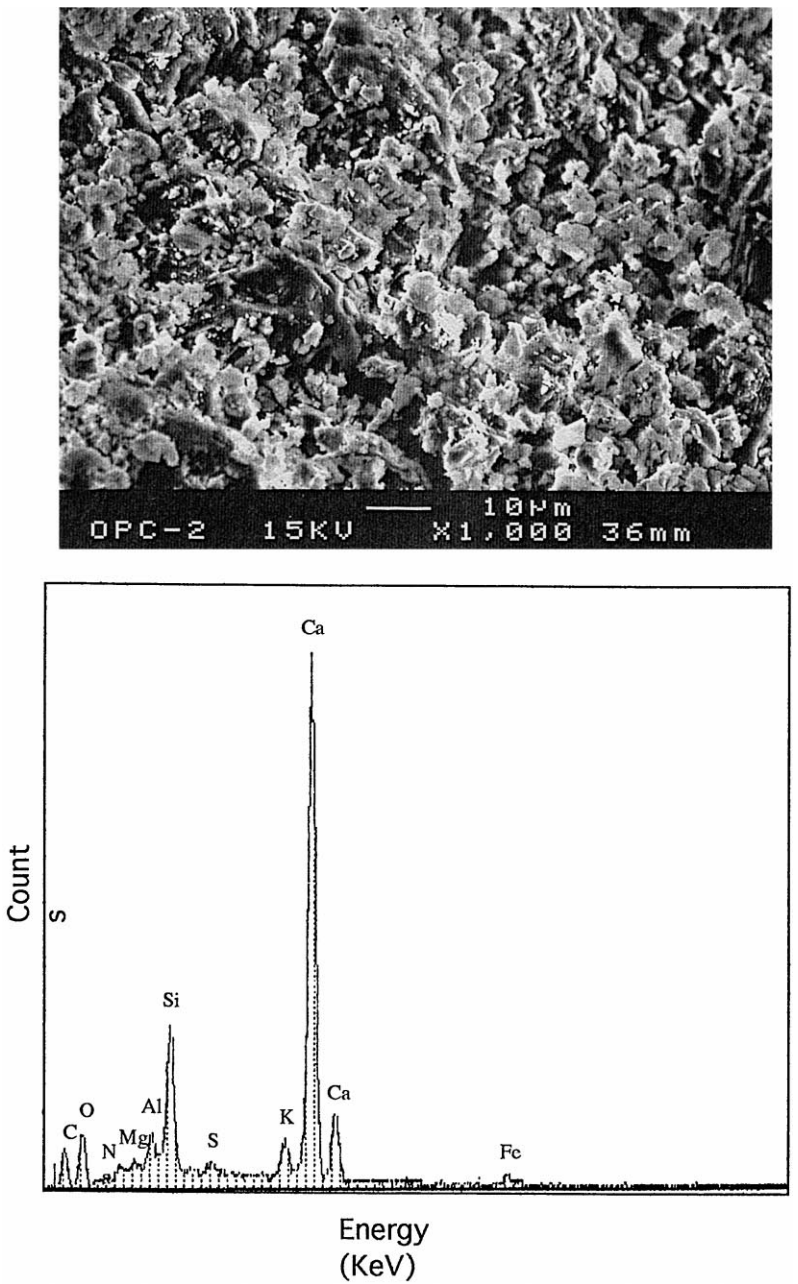

Fig. 3. SEM image (×1000) and EDS spectrum (×1000) of OPC-V.

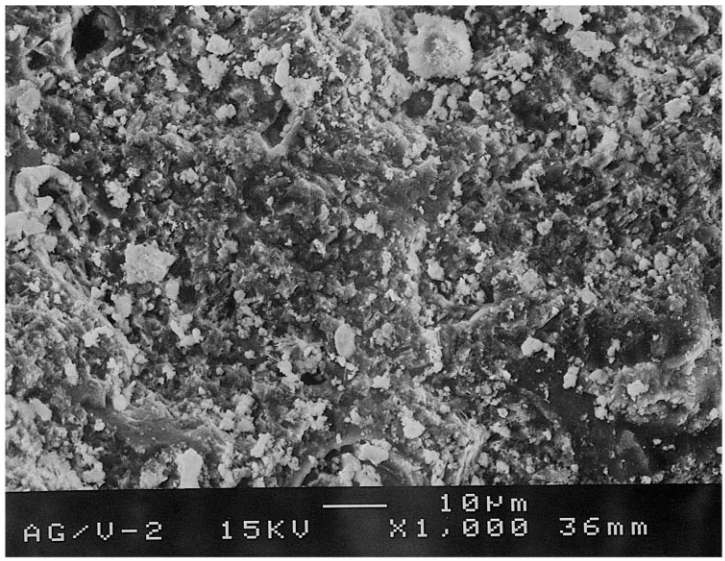

(a)

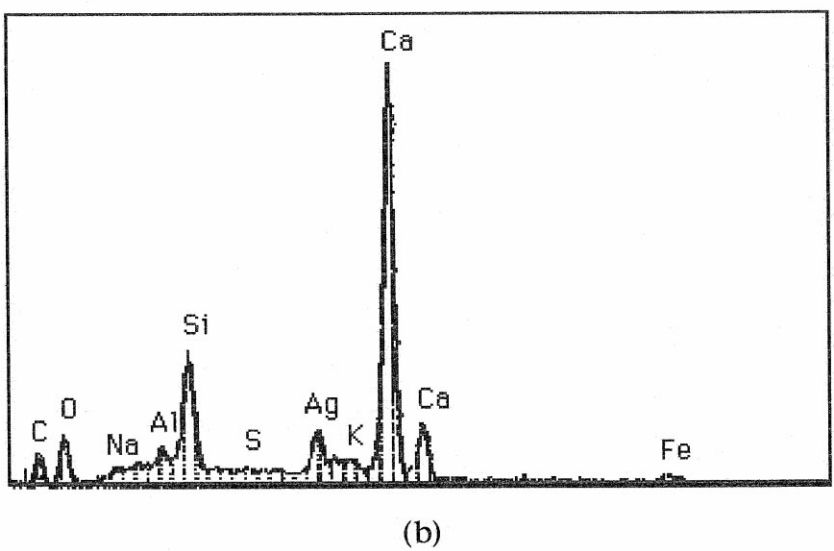

(b)

Fig. 4. SEM image (×1000) and EDS spectrum (×1000) of OPC-V/Ag (area 1).

sodium (trace), magnesium (trace) and iron (trace). An additional peak due to Ag is also observed. It is interesting to note that the potassium peak intensity has been reduced due to the presence of Ag^+ in the matrix. Since EDS is not purely a surface sensitive technique and has a penetration of >1 μm [18], it is believed that Ag^+ has been

ion-exchanged with K^+. However, the mechanism of this ion exchange reaction is not clearly understood. The preponderance of the silver instead of potassium can be explained by preferential adsorption in which the Ag^+ cations compete with other cations in the pore water system. A set of equilibrium reactions may be presumed in competition with cations, such as H^+, Na^+, K^+, Ca^{2+} and waste Ag^+ ions [19]. In addition to adsorption, the direct precipitation of Ag_2O and $Ag(OH)_2$ may also take

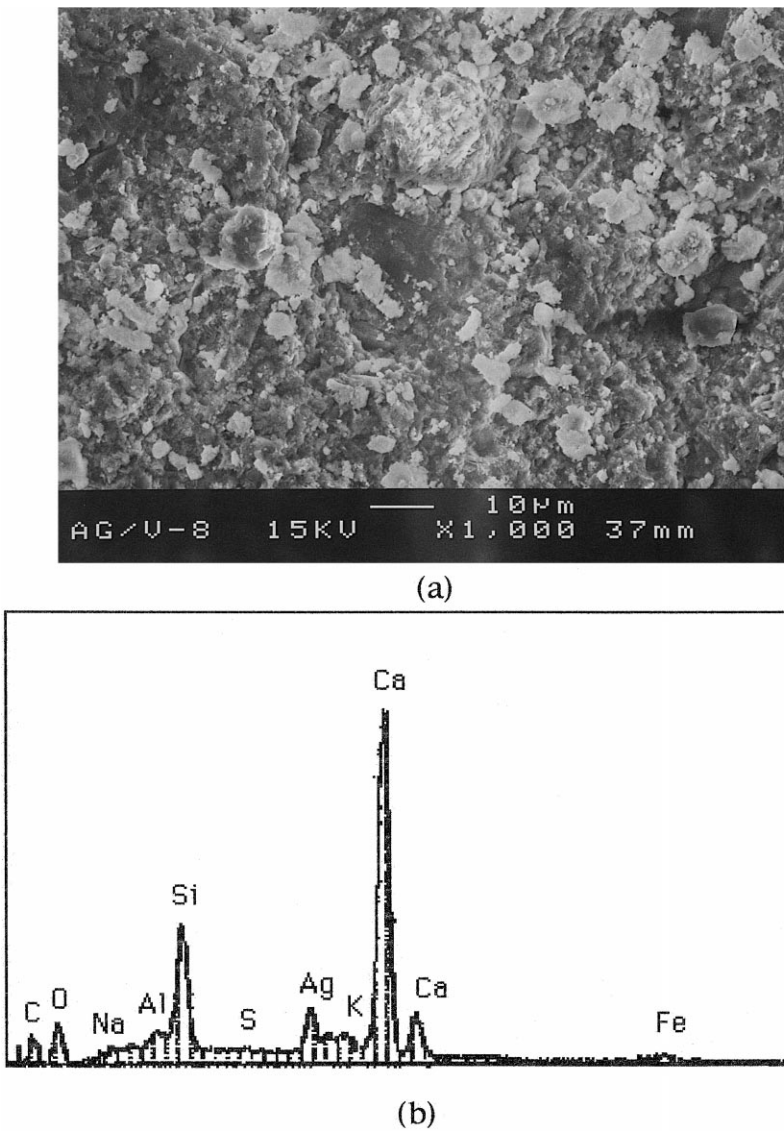

Fig. 5. SEM image (×1000) and EDS spectrum (×1000) of OPC-V/Ag (area 3).

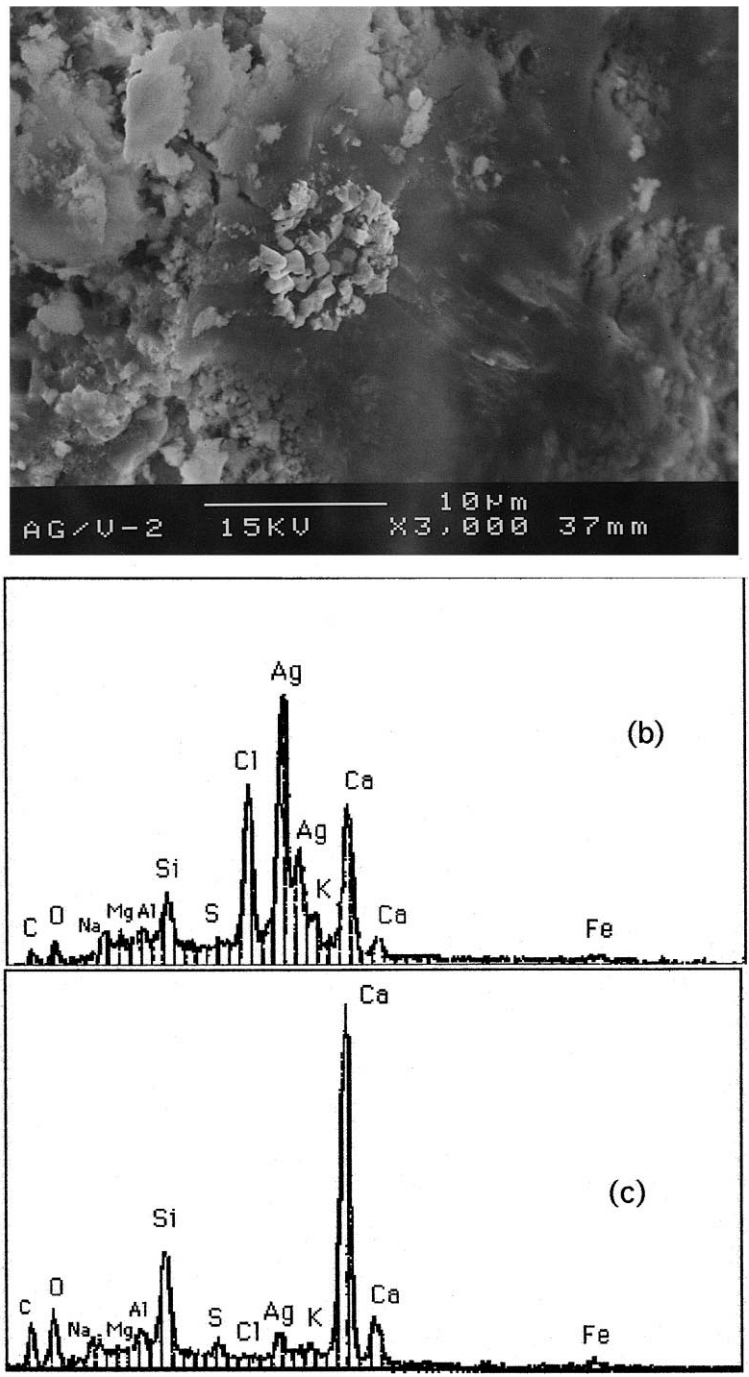

Fig. 6. (a) SEM image of OPC-V/Ag (area 4); EDS spectrum of light area (b) and dark area (c) at ×300,000.

place along with the expected reactions. The Ag^+ ions may also be in competition with CH and C–S–H for reactions with CO_2 to form Ag_2CO_3.

The SEM image ($\times 1000$) of a different area (area 2) and the corresponding EDS spectrum (Fig. 5) reveal some significant features. Close examination of Fig. 5 reveals that clusters of compounds are present in OPC-V/Ag and the calcium to silicon ratio (Ca/Si) is relatively lower than that in area 1.

A magnified SEM image ($\times 3000$) of OPC-V/Ag (area 3) is presented in Fig. 6, and it clearly indicates the presence of a cluster of crystalline compounds in the OPC-V/Ag sample area under consideration. The EDS examination of area 'a'—cluster area, (Fig. 6b) establishes the presence of chlorine along with silver. Another EDS scan of the darker area (area 'b') is shown in Fig. 6c. Examinations of Fig. 6b and c clearly demonstrate that the cluster (area 'a') contains much more Ag^+ and Cl^- containing compounds as compared with area 'b'. The relative intensities of the Ca and Si peaks are also significantly different. The cluster (Fig. 6a) is presumably composed of AgCl crystals. The appearance of the AgCl cluster in OPC-V/Ag system is a significant observation. Chloride ions in cement may be introduced as an impurity from chloride bearing aggregates, water and the admixtures used. A knowledge of the speciation of chloride in concrete is important, since its presence in steel reinforced concrete structures causes pitting corrosion even though the pH of the medium is greater than 11.0 [20]. The mechanism of formation of AgCl is discussed in the following section.

4. Speciation of Ag in cementitious environment

The speciation of Ag^+ ions in an alkaline and high ionic strength environment like cement paste (pH = 12.5–13.0) and their speciation is presented in Fig. 7. Both the acid–base and redox solution chemistry of silver must be considered to explain Fig. 7. Reaction (1) shows the redox reactions of silver.

$$Ag^{3+} \; e^- \underset{\text{oxidation}}{\overset{\text{reduction}}{\rightleftarrows}} Ag^{2+} + e^- \underset{\text{oxidation}}{\overset{\text{reduction}}{\rightleftarrows}} Ag^{1+} + e^- \underset{\text{oxidation}}{\overset{\text{reduction}}{\rightleftarrows}} Ag^0 \tag{1}$$

In the present experiment, 10% Ag^+ ions (2.6 M Ag in water) was added to cement at a w/c ratio of 0.35. The oxidized state of silver in the cement-paste environment can be predicted from a knowledge of $pE = \{-\log [e^-]\}$ of the aqueous medium, since pE describes the equilibrium position for all redox pairs (ox/red) in a particular system. The pE of the hydrating cement system was calculated from a knowledge of the concentration of atmospheric oxygen and pH of the system assuming oxygen as the potential establishing species [21]. Thus considering the oxidation reaction:

$$1/4O_2 + H^+ + e^- \Leftrightarrow 1/2H_2O \tag{2}$$

the pE for reaction (2) was derived from the Nernst Equation,

$$pE = pE^0 + \log\left\{(PO_2)^{1/4} a_{H^+}\right\} \tag{3}$$

$$pE = 20.75 - pH \tag{4}$$

where $PO_2 = 0.2029$ atm in neutral water (25°C) in equilibrium with $pE = 8.077$ [22]. Therefore, $E = 0.05916 \cdot pE = 0.478$ V.

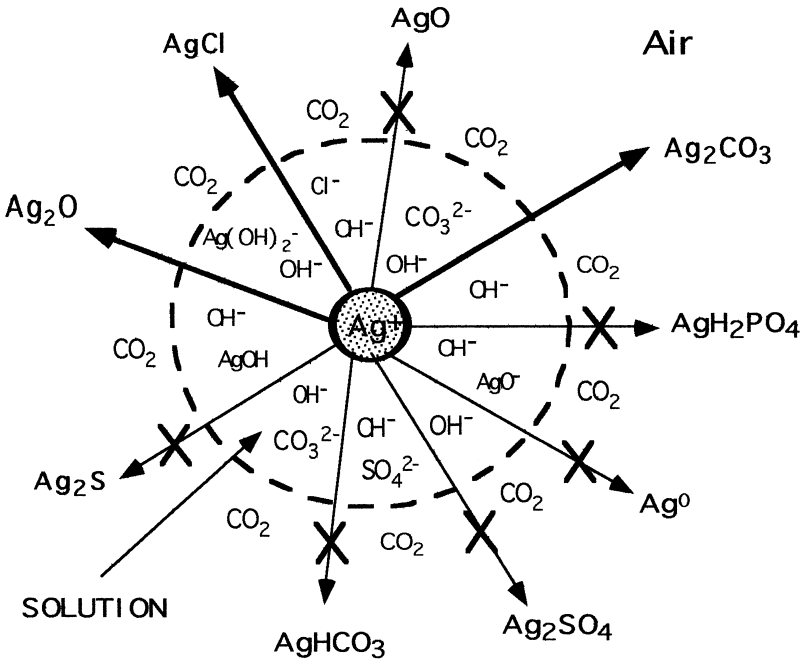

Fig. 7. Potential silver species in cementitious environment *x*—means chemically not likely to form. Highlighted arrow means chemically stable species.

This result, combined with the pH vs. $E/(\mathrm{V})$ stability diagram [23] for the Ag–water system, clearly indicates that at pH = 12.0–13.0 and $E/(\mathrm{V}) = 0.478$ (or $\mathrm{p}E = 8.077$) the most stable silver compound is Ag_2O and the equilibrium concentration of Ag^+ is about 10^{-4} M. AgO^- and Ag^0 are not expected to be present in this pH–pE range. AgH_2PO_4 is unlikely to form, since no phosphorous species are present in cement clinkers. $AgHCO_3$ cannot be formed at such a high pH condition, since HCO_3^- is not present. Ag_2S is also unlikely to be formed, since gypsum is the only source of sulfur (S^{2-}), and no sulfide (S^-) species are expected in the cement system. It is, therefore, concluded that the possible silver species in the cement environment are Ag^{1+} compounds which may include: Ag_2O, AgCl, Ag_2CO_3 and Ag_2SO_4. Here, the later is unlikely because of its relatively high solubility. The sequence of reactions for the formation of the first three stable Ag^{1+} compounds are:

$$2Ag^+ + 3OH^- \Leftrightarrow AgOH + Ag(OH)_2^- \rightarrow Ag_2O\downarrow(\text{solid}) + H_2O + OH^- \quad (5)$$

$$AgO^- + Ag^+ + CO_2 \Leftrightarrow Ag_2CO_3\downarrow(\text{solid}) \quad (6)$$

$$Ag^+ + Cl^- \Leftrightarrow AgCl\downarrow(Solid) \quad (7)$$

The K_{sp} ($=[Ag^+]^2[OH^-]^2$) of Ag_2O in aqueous solution calculated from the equilibrium reaction: $Ag_2O + H_2O \Leftrightarrow 2Ag^+ + 2OH^-$ is 10^{-12}, since in the present case, $[Ag^+] = 10^{-4}$ M and $[OH^-] = 10^{-2}$ at pH = 12. The K_{sp} values of Ag_2CO_3, AgCl and Ag_2SO_4 are 8.45×10^{-12}, 1.77×10^{-10} and 1.20×10^{-5}, respectively [24].

It can be seen that the solubility of Ag_2SO_4 is much higher than Ag_2O, Ag_2CO_3 and AgCl. Therefore, as stated above, Ag_2SO_4 is very unlikely to be found in the cement system as well as in pore water.

The least soluble Ag_2CO_3 and AgCl compounds will precipitate from the pore solution. The rate of precipitation increases with the progress of hydration, since the hydration reaction removes water from the pore solution and consequently increase the concentration of Ag^+ and Cl^- ions in the system. The formation of the cluster of AgCl is preceded by the nucleation of AgCl at the CSH surface in the pore solution. Ag_2CO_3 may also be formed and co-exist with AgCl and Ag_2O. However, due to limited amounts of CO_3^{2-} in the system at the early stages of hydration, Ag_2CO_3 should not be found as much as the other two species in cement paste. Indications of the presence of Ag_2CO_3 also comes from FT-IR and XRD examinations of the OPC-V/Ag samples.

However, the formation of AgCl clusters is critically controlled by a particular micro-situation in the pore solution and nucleation and growth of AgCl. The formation of AgCl clusters at the cement surface is possibly caused by the localization of Ag^+ and Cl^- ions in the pore solution. The formation of clusters of AgCl crystals as seen in SEM images from the reactions between Ag^+ and Cl^- ions is preceded by nucleation of this compound at the gel membrane surface. It appears that the AgCl forms after most of the CSH has been deposited. The growth of well formed AgCl crystals means that the process was in extended steady state with the local pore solution and allowed Ag^+ to be transported to the nucleating AgCl sites. The AgCl clusters may assume Ag^1 (d^{10}) octahedral geometry as in the case of NaCl structure. There were still small amounts of Ag species found in all areas, indicating the presence of amorphous surface Ag_2O and Ag_2CO_3 or its encapsulated analogs. It is hard to determine experimentally whether these small amounts of Ag^+ species are present as Ag_2O or Ag_2CO_3, but chemical logic and equilibrium models suggest their presence.

5. Conclusions

The presence of Ag^+ ions did not significantly affect the silicate environment in a hydrating cement system. The characterization of the silver doped cement samples by XRD indicated that AgCl, Ag_2CO_3 and Ag_2O are formed in a cementitious environment. The formation of the silver species are critically controlled by a particular micro-situation in the pore solution. Silver chloride clusters were identified by SEM/EDS analyses of the OPC-V/Ag samples. The AgCl cluster in cementitious system is formed by precipitation preceded by nucleation in the pore solution.

Acknowledgements

The authors acknowledge financial support from the Gulf Coast Hazardous Substances Research Center, Project 104LUB0437, Lamar University, Beaumont, TX and The Robert A. Welch Foundation (Houston, TX). This material is also based in part upon work supported by the Texas Advanced Research (Technology) Program under Grant No. 003658-344.

References

[1] Toxic Chemical Release Reporting; Community Right-to-Know Act, USEPA (52 FR 21152) (1987).
[2] L.S. Goodman, A. Gilman (Eds.), The Pharmacological Basis of Therapeutics, 5th edn., MacMillan Publ., NY (1975).
[3] Ambient Water Quality Criteria for Silver, U.S. Environmental Protection Agency, EPA 400/5-80-071 (1980).
[4] R.D. Spence (Ed.), Microstructure of Solidified Waste Forms, Lewis Publishers, USA (1993).
[5] R.E. Landreth, Guide to the Disposal of Chemically Stabilized and Solidified Wastes, EPA SW-872, U.S. EPA, Cincinnati, OH (1980).
[6] R.B. Pojasek (Ed.), Toxic and Hazardous Waste Disposal, Vols. 1 and 2, Ann Arbor Sci., Ann Arbor, MI (1979).
[7] C.C. Wiles, A review of solidification/stabilization technology, J. Hazardous Materials 14 (1987) 5–21.
[8] C.D. Hills, C.J. Sollars, R. Perry, Ordinary Portland cement based solidification of toxic wastes: the role of OPC reviewed, Cement Concr. Res. 23 (1993) 19.
[9] M.Y.A. Mollah, Y.N. Tsai, T.R. Hess, D.L. Cocke, An FTIR, SEM and EDS investigation of solidification/stabilization of chromium using Portland cement type V and type IP, J. Hazardous Materials 30 (1992) 273–283.
[10] M.Y.A. Mollah, P. Palta, T.R. Hess, R.K. Vempati, D.L. Cocke, Chemical and physical effects of lignosulfonate superplasticizer on the hydration of Portland cement and solidification/stabilization consequences, Cement Concr. Res. 25 (3) (1995) 671–682.
[11] M.Y.A. Mollah, Y.-N. Tsai, T.R. Hess, D.L. Cocke, An FTIR investigation of cement based solidification/stabilization system doped with cadmium, J. Environ. Sci. Health 27 (5) (1992) 1213–1227.
[12] L.G. Berry (Ed.), Inorganic Index to the Powder Diffraction File, PA, JCPDS (1974).
[13] W.F. Cole, B. Kroone, Carbon dioxide in hydrated Portland cement, J. Am. Concr. Inst. 31 (1960) 1275.
[14] M.Y.A. Mollah, J.R. Parga, D.L. Cocke, An infrared spectroscopic examination of cement-based solidification/stabilization systems—Portland type V and IP with zinc, J. Environ. Sci. Health A 27 (6) (1992) 1503–1519.
[15] V.C. Farmer, The Infrared Spectra of Minerals, Mineralogical Soc., London (1974).
[16] R.G.J. Strens, The chain, ribbon and ring silicates, in: V.C. Farmer (Ed.), The Infrared Spectra of Minerals, Mineralogical Soc., London (1974).
[17] S.N. Ghosh, S.K. Handoo, Infrared and Raman studies in cement and concrete, Cement Concr. Res. 10 (1980) 771–782.
[18] H.G. McWhinney, D.L. Cocke, L.K. Blake, J.D. Ortego, An investigation of mercury solidification and stabilization in Portland cement using X-ray photoelectron spectroscopy and energy dispersive spectroscopy, Cement Concr. Res. 20 (1) (1990) 79–91.
[19] D.L. Cocke, M.Y.A. Mollah, The Chemistry and Leaching Mechanisms of Hazardous Substances in Cementious Solidification/Stabilization Systems, Chemistry and Microstructure of Solidified Waste Form, Lewis Publ., Boca Raton, USA (1993).
[20] M.N. Haque, O.A. Kayyali, Free and Water Soluble Chloride in Concrete 25 (3) (1995) 531–542.
[21] J.F. Pankow, Aquatic Chemistry Concepts, Lewis Publishers, MI (1991).
[22] S.E. Manahan, Environmental Chemistry, 5th edn., Lewis Publ. (1990).
[23] G. Charlot, L'analyse Qualitative et les reactions en Solution, 4th edn., Masson, Paris (1957).
[24] D.R. Lide, CRC Handbook of Chemistry and Physics, 75th edn., CRC Press, Boca Raton, FL (1994).